

Global oscillation analysis of solar neutrino data with helioseismically constrained fluxes

Sandhya Choubey^{1*}, Srubabati Goswami^{1†}, Kamales Kar^{1‡}, H.M. Antia^{2§}, S.M. Chitre^{2,3**}

¹*Saha Institute of Nuclear Physics, 1/AF, Bidhannagar, Kolkata 700 064, India*

²*Tata Institute of Fundamental Research, Homi Bhabha Road, Mumbai 400005, India*

³*Queen Mary and Westfield College, Mile End Road, London E1 4NS, U. K.*

Abstract

A seismic model for the Sun calculated using the accurate helioseismic data predicts a lower ^8B neutrino flux as compared to the standard solar model (SSM). However, there persists a discrepancy between the predicted and measured neutrino fluxes and it seems necessary to invoke neutrino oscillations to explain the measurements. In this work, we have performed a global, unified oscillation analysis of the latest solar neutrino data (including the results of SNO charged current rate) using the seismic model fluxes as theoretical predictions. We determine the best-fit values of the neutrino oscillation parameters and the χ^2_{\min} for both $\nu_e - \nu_{\text{active}}$ and $\nu_e - \nu_{\text{sterile}}$ cases and present the allowed parameter regions in the $\Delta m^2 - \tan^2 \theta$ plane for $\nu_e - \nu_{\text{active}}$ transition. The results are compared with those obtained using the latest SSM by Bahcall and his collaborators.

PACS: 14.60.Pq, 12.15.Ff, 26.65.+t, 96.60.Ly

I. INTRODUCTION

Solar neutrino fluxes measured by all the experiments to date are significantly at variance with the expected theoretical predictions. The most recent confirmation of this has come from the heavy water (D_2O) detector at Sudbury Neutrino Observatory (SNO) [1] which measures the solar ^8B neutrinos through the charged current (CC) reaction $\nu_e d \rightarrow p p e^-$. SNO has also published their result of ^8B flux measured by the neutrino-electron scattering

*e-mail: sandhya@theory.saha.ernet.in

†e-mail: sruba@theory.saha.ernet.in

‡e-mail: kamales@tnp.saha.ernet.in

§e-mail: antia@astro.tifr.res.in

**e-mail: chitre@astro.tifr.res.in

reaction (ES) and reported a lower ^8B flux as compared to theoretical predictions of the standard solar model. This is in agreement with the ^8B flux measured by the SuperKamiokande (SK) detector through the same reaction [2]. Thus, SNO and SK confirm the deficit of solar neutrino fluxes reported first in the ^{37}Cl radiochemical experiment of Davis *et al.* [3] and subsequently by Kamiokande [4] and the radiochemical ^{71}Ga experiments SAGE, GALLEX and GNO [5]. The theoretical predictions most widely used are from the standard solar model (SSM) developed and remarkably refined over the last four decades by Bahcall and his collaborators [6–8]. In recent years, the observations of solar oscillations have provided an independent test of solar models. Inversions of accurately measured frequencies of solar oscillations have enabled a determination of the sound speed and density profiles inside the Sun [9]. While the SSM matches these inverted profiles remarkably well, there is still a significant discrepancy which is much larger than the errors in helioseismic inversions. It would, therefore, be desirable to check the results on neutrino oscillation solutions to the solar neutrino problem using a solar model which is consistent with the helioseismic data. Such models can be constructed using the inverted profiles of sound speed and density along with the equations of thermal equilibrium, provided the heavy element abundance profile and the input physics like opacity, equation of state and nuclear reaction rates are assumed to be known [10,11]. These models represent the present Sun and do not depend on evolutionary history of the Sun. Such seismic models can be used to calculate solar neutrino fluxes which turn out to be somewhat different from those obtained with the standard solar model.

In this work, we consider the seismic model calculated using the technique described by Antia and Chitre [11], but using updated helioseismic data. This model predicts a lower ^8B flux than the BP2000 SSM [8]. However, when all the experimental rates are taken together there is still inconsistency between theory and experiment [11]. This inconsistency cannot be removed even if opacities and heavy element abundances are varied by arbitrarily large amount [12]. Thus one needs to invoke neutrino oscillations to explain the observed fluxes of solar neutrinos. Seismic models have also provided some constraints on the pp reaction cross-section [11,13–15]. It appears that pp reaction cross-section needs to be increased by about 4% over the value used by Bahcall *et al.* [8], to obtain solar models that are consistent with seismic data. This increase in pp reaction rate in the seismic model with correct luminosity tends to decrease the predicted neutrino fluxes for all four experiments.

In addition to the data on the total flux, SK also provides the data on the day-night recoil electron energy spectrum [16] and the zenith angle distribution of events [17]. SNO has also reported the recoil electron energy spectrum for the CC events. Global oscillation analysis of the data on rates and spectrum has been carried out by different groups to put constraints on the oscillation parameters [18–23] (pre-SNO) and [24–27] (post-SNO). These studies have used the neutrino fluxes from the standard solar model of Bahcall *et al.* [7,8]. However, it would be interesting to see the implications of neutrino fluxes from the seismic model on the oscillation parameters. In this work, we perform a global and unified oscillation analysis of the solar neutrino data on total fluxes from the SNO, Cl, Ga and SuperKamiokande experiments together with the day-night spectrum data from SK using the seismically inferred neutrino fluxes and compare the results with those obtained using

the latest standard solar model (BP2000) of Bahcall *et. al.* [8]¹. We use the latest 1258-day SK data in our analysis [28].

The rest of the paper is organized as follows: in section 2 we present the basic features of the seismic model and describe the formalism for the unified analysis in Section 3. In section 4 we discuss the procedure for the analysis and the results and finally, summarize the conclusions in Section 5.

II. THE SEISMIC MODEL

We use the mean frequencies from the Michelson Doppler Imager (MDI) data from the first 360 days of its operation [29], to calculate the sound speed and density profiles inside the Sun using a regularized least squares inversion technique [30]. We adopt the inverted sound speed and density profiles, along with the heavy element abundance (Z) profile from the solar model of [31] to calculate the seismic model using equations of thermal equilibrium [11]. We use the OPAL opacities [32] and equation of state [33], and nuclear reaction rates from [34], except for the proton-proton reaction rate, which is slightly adjusted to yield the correct observed solar luminosity [14]. With the latest physical and seismic input, the pp reaction cross-section S_{11} needs to be increased to 4.17×10^{-25} MeV barns. The helium abundance by mass at the base of the convection zone in this seismic model turns out to be 0.250, which is in good agreement with the helioseismic estimate in the envelope [35].

With the knowledge of temperature, density and composition profiles from the seismic model, neutrino fluxes can be calculated and the results are shown in Table I. Apart from inversion errors, other main sources of uncertainties in these calculated fluxes are the nuclear reaction cross-sections for the ^3He - ^3He ($S_{3,3}$), ^3He - ^4He ($S_{3,4}$), p - ^{14}N ($S_{1,14}$), p - ^7Be ($S_{1,7}$) reactions, as well as the solar luminosity, the heavy element abundance, Z and opacities, κ . To estimate the effect of these quantities on neutrino fluxes in the seismic model we calculate the logarithmic derivatives of neutrino fluxes with respect to each of these quantities (X_i) and these are also listed in Table I, with the last row showing the estimated relative errors in these quantities. Apart from these we also include the uncertainty due to the electron capture rate of the process $^7\text{Be}(e^-, \nu_e)^7\text{Li}$ and the astrophysical uncertainty in the S_0 factor of the reaction $^{16}\text{O}(p, \gamma)^{17}\text{F}$. These contributions are same as in [8]. The expected neutrino fluxes in various solar neutrino experiments can be calculated from Table I and these values are given in Table II, for comparison with observed fluxes [3,5,28] and those in the standard solar models [8,7,36,37]. In Table III we present the contributions of the various neutrino sources to the Cl and Ga experiments according to the seismic model and BP2000. Table IV summarises the ratios of the experimental rates to the theoretical predictions for the Cl, Ga, SK and SNO experiments for both BP2000 and seismic model. For SNO we display only the CC rate. We also show the compositions of major flux components.

The neutrino fluxes in our seismic model are somewhat different from those in the seismic model of Watanabe and Shibahashi [38]. The main difference arises because they have used

¹We have not incorporated the SNO ES data as well as the SNO CC spectrum data as they still have large errors.

only the sound speed from primary inversions to calculate the seismic model, while we have used both sound speed and density profiles from primary inversions. Thus the density profile in seismic model of Watanabe and Shibahashi does not, in fact, match the inverted density profile. Further, since the density profile in their model is not constrained to seismic profile they are able to construct seismic model with correct luminosity using the standard pp nuclear reaction rate, which tends to give larger neutrino fluxes. If they were to assume a slightly larger cross-section for pp reaction, the density profile in their model would be in better agreement with the inverted profile. Apart from this, the adopted heavy element abundance, Z -profile is also different in their work. While we have taken the Z -profile from model of Richard et al. [31], which includes mixing just below the base of convection zone, as implied by helioseismic data [39,9], Watanabe and Shibahashi [38] use a homogeneous Z profile. Similarly, the neutrino fluxes in our seismic model are somewhat smaller than those in SSM [8]. The main reasons for this reduction are again the increase in S_{11} and neglect of mixing just beneath the convection zone in SSM. If these had been incorporated, then the SSM fluxes should also come close to the corresponding seismic model fluxes.

III. FORMALISM FOR UNIFIED OSCILLATION ANALYSIS

The general expression for the probability amplitude of survival for an electron neutrino produced in the deep interior of the Sun, for two neutrino flavors, is given by [40]

$$A_{ee} = A_{e1}^{\odot} A_{11}^{\text{vac}} A_{1e}^{\oplus} + A_{e2}^{\odot} A_{22}^{\text{vac}} A_{2e}^{\oplus} \quad (1)$$

where $A_{ek}^{\odot} (k = 1, 2)$ gives the probability amplitude of $\nu_e \rightarrow \nu_k$ transition at the solar surface, A_{kk}^{vac} is the survival amplitude from the solar surface to the surface of the Earth and A_{ke}^{\oplus} denotes the $\nu_k \rightarrow \nu_e$ transition amplitudes inside the Earth. We can express

$$A_{ek}^{\odot} = a_{ek}^{\odot} e^{-i\phi_k^{\odot}} \quad (2)$$

where ϕ_k^{\odot} is the phase picked up by the neutrinos on their way from the production point in the central regions to the surface of the Sun and

$$a_{e1}^{\odot 2} = \frac{1}{2} + \left(\frac{1}{2} - P_J\right) \cos 2\theta_m \quad (3)$$

θ_m being the mixing angle at the production point of the neutrino, given by

$$\tan 2\theta_m = \frac{\Delta m^2 \sin 2\theta}{\Delta m^2 \cos 2\theta - 2\sqrt{2}G_F n_e E}. \quad (4)$$

Here n_e is the ambient electron density, E the neutrino energy, and $\Delta m^2 (= m_2^2 - m_1^2)$ is the mass squared difference in vacuum. We denote by P_J the non-adiabatic level jumping probability between the two mass eigenstates which for an exponential density profile² can be expressed as [41]

²Note that for the actual calculation of the probabilities we have used the numerical density profile given in [8] for SSM and the model in [11] with updated helioseismic data for seismic model.

$$P_J = \frac{\exp(-\gamma \sin^2 \theta) - \exp(-\gamma)}{1 - \exp(-\gamma)} \quad (5)$$

$$\gamma = \pi \frac{\Delta m^2}{E} \left| \frac{d \ln n_e}{dr} \right|_{r=r_{res}}^{-1} \quad (6)$$

For sterile neutrinos, the n_e in Eq. (4) has to be replaced by $n_e - \frac{1}{2}n_n$, where n_n is the neutron number density. The survival amplitude A_{kk}^{vac} is given by

$$A_{kk}^{\text{vac}} = e^{-iE_k(L-R_\odot)} \quad (7)$$

where E_k is the energy of the state ν_k , L is the distance between the center of the Sun and Earth and R_\odot is the solar radius. For a two-slab model of the Earth — a mantle and core with constant densities of 4.5 and 11.5 gm cm⁻³ respectively, the expression for A_{2e}^\oplus can be written as (assuming the flavor states to be continuous across the boundaries) [42]

$$A_{2e}^\oplus = \sum_{\substack{i,j,k, \\ \alpha,\beta,\sigma}} U_{ek}^M e^{-i\psi_k^M} U_{\alpha k}^M U_{\alpha i}^C e^{-i\psi_i^C} U_{\beta i}^C U_{\beta j}^M e^{-i\psi_j^M} U_{\sigma j}^M U_{\sigma 2} \quad (8)$$

where (i, j, k) denotes mass eigenstates and (α, β, σ) denotes flavor eigenstates, U , U^M and U^C are the mixing matrices in vacuum, in the mantle and the core respectively and ψ^M and ψ^C are the corresponding phases picked up by the neutrinos as they travel through the mantle and the core of the Earth. The ν_e survival probability is given by

$$\begin{aligned} P_{ee} &= |A_{ee}|^2 \\ &= a_{e1}^{\odot 2} |A_{1e}^\oplus|^2 + a_{e2}^{\odot 2} |A_{2e}^\oplus|^2 \\ &\quad + 2a_{e1}^{\odot} a_{e2}^{\odot} \text{Re}[A_{1e}^\oplus A_{2e}^{\oplus *} e^{i(E_2-E_1)(L-R_\odot)} e^{i(\phi_{2,\odot}-\phi_{1,\odot})}] \end{aligned} \quad (9)$$

Identifying $P_\odot = a_{e1}^{\odot 2}$ and $P_\oplus = |A_{1e}^\oplus|^2$ Eq. (9) can be expressed as [43,44,40]

$$P_{ee} = P_\odot P_\oplus + (1 - P_\odot)(1 - P_\oplus) \quad (10)$$

$$+ 2\sqrt{P_\odot(1 - P_\odot)P_\oplus(1 - P_\oplus)} \cos \xi \quad (11)$$

where we have combined all the phases involved in the Sun, vacuum and inside Earth in ξ . This is the most general expression for survival probability for the unified analysis of solar neutrino data. Depending on the value of $\Delta m^2/E$ one recovers the well known *Mikheyev-Smirnov-Wolfenstein* (MSW) [45] and vacuum oscillation (VO) [46] limits:

- In the regime $\Delta m^2/E \lesssim 5 \times 10^{-10}$ eV²/MeV matter effects inside the Sun suppress flavor transitions and $\theta_m \approx \pi/2$. Therefore, from (3), we obtain $P_\odot \approx P_J \approx \cos^2 \theta$ as the propagation of neutrinos is extremely non-adiabatic and likewise, $P_\oplus = \cos^2 \theta$ to give

$$P_{ee}^{\text{vac}} = 1 - \sin^2 2\theta \sin^2(\Delta m^2 (L - R_\odot)/4E) \quad (12)$$

- For $\Delta m^2/E \gtrsim 10^{-8} \text{ eV}^2/\text{MeV}$, the total oscillation phase becomes very large and the $\cos \xi$ term in Eq. (11) averages out to zero. One then recovers the usual MSW survival probability

$$P_{ee}^{\text{MSW}} = P^D + \frac{(2P^D - 1)(\sin^2 \theta - |A_{2e}^\oplus|^2)}{\cos 2\theta} \quad (13)$$

The day-time probability is given by P^D being

$$P^D = \frac{1}{2} + \left(\frac{1}{2} - P_J\right) \cos 2\theta \cos 2\theta_m \quad (14)$$

- In between the *pure* vacuum oscillation regime where the matter effects can be safely neglected, and the *pure* MSW zone where the coherence effects due to the phase ξ can be conveniently disregarded, is a region where both effects can contribute. For $5 \times 10^{-10} \text{ eV}^2/\text{MeV} \lesssim \Delta m^2/E \lesssim 10^{-8} \text{ eV}^2/\text{MeV}$, both matter effects inside the Sun and coherent oscillation effects in the vacuum become important. This is the *quasi vacuum oscillation* (QVO) regime [40]. In this region, $P_\odot \approx P_J$ and $P_\oplus = \cos^2 \theta$ and the survival probability is given by [43,47]

$$P_{ee} = P_J \cos^2 \theta + (1 - P_J) \sin^2 \theta + \sin^2 2\theta \sqrt{P_J(1 - P_J)} \cos \xi \quad (15)$$

we calculate P_J in this region using the prescription given in [47].

IV. RESULTS AND DISCUSSIONS

In this section we present our results of global χ^2 -analysis of the data on total rates and the day-night spectrum observed in SK. We have done two sets of calculations taking the theoretical predictions from the seismic model as well as from BP2000 SSM. Our principal objective is to compare the two sets of results.

Different approaches have been adopted regarding the treatment of the SK data on total rates and the recoil electron energy spectrum, in the global analysis. A critical comparison of the various methods used and the dependence of the final results on the method followed is discussed in a lucid and extensive manner in [22]. Below we summarise the salient features.

- (i) One approach is to include both the SK rate and the spectrum in the global analysis [21,22].
- (ii) The total rate measured in SK is not independent of the spectrum and hence the above method of including both may lead to a possible overcounting of events. To avoid this the total SK rate is excluded from the global analysis in [22,25].
- (iii) Another approach adopted to avoid the overcounting is to include the total SK rate in the global analysis but to adopt a free normalization factor for the spectrum [19,22–24,26]. Thus the spectrum gives information on only the shape of the ^8B survival probability.

In case of methods (i) and (ii), if the ^8B flux normalisation is varied as a free parameter in both rates and spectrum, no error correlation between these needs to be taken [22]. On the other hand, if the ^8B flux normalisation is kept fixed at the SSM value, then one should incorporate the correlation between the error in the ^8B flux measured in the total rates and the SK spectrum [21,25]. For method (iii), since the normalisation of the spectrum is varied as a free parameter, the χ^2 due to rates and spectrum can be summed independently. For the purpose of this paper we adopt method (iii), so that our total χ^2 is given by

$$\chi_{\text{total}}^2 = \chi_{\text{rates}}^2 + \chi_{\text{spectrum}}^2 \quad (16)$$

where

$$\chi_{\text{rates}}^2 = \sum_{i,j} \left(F_i^{\text{th}} - F_i^{\text{exp}} \right) (\sigma_{ij}^{-2}) \left(F_j^{\text{th}} - F_j^{\text{exp}} \right). \quad (17)$$

Here $F_i^\xi = T_i^\xi / T_i^{\text{SSM}}$, where ξ designates *th* (for the theoretical prediction with oscillations) or *exp* (for the experimental value) and T_i stand for the quantities total rates from different experiments. We have used the weighted average of the three Ga experimental rates and thus we have 4 data points for the total rates. The error matrix σ_{ij} contains the experimental errors, theoretical errors and their correlations. The correlation matrix for the total rates is constructed as in [50]. The logarithmic derivatives for the seismic model needed for the calculation of error correlation matrix are given in Table I. For the SSM we take the latest values from [8]. The spectrum chi-square is defined as,

$$\chi_{\text{spectrum}}^2 = \sum_{i,j} \left(X_{\text{sp}} F_i^{\text{th}} - F_i^{\text{exp}} \right) (\sigma_{ij}^{-2}) \left(X_{\text{sp}} F_j^{\text{th}} - F_j^{\text{exp}} \right). \quad (18)$$

Here $F_i^\xi = S_i^\xi / S_i^{\text{SSM}}$ where ξ designates *th* (for the theoretical prediction with oscillations) or *exp* (for the experimental value) and S_i stands for the electron energy spectrum for different energy bins. We have used 1258 day SK data on the electron energy spectrum at day and night which includes the energy bin from 5.0-5.5 MeV also and we have 38 data points for the spectrum. X_{sp} is the normalisation factor for the spectrum which is floated as a free parameter in the global analysis in order to filter out the information on the total flux from the spectrum data. Thus for the global analysis we have 41 degrees of freedom (DOF) for the no oscillation scenario. For the error matrix in the spectrum data we include the statistical error, correlated and uncorrelated systematic errors and the error due to the calculation of the spectrum [16]. The no oscillation χ_{min}^2 for 41 DOF for BP2000 SSM is 89.27 while for the seismic model it is 94.17.

Next, we perform the chi-square analysis assuming neutrino oscillations to operate. For the oscillation analysis, there are two parameters – Δm^2 and $\tan^2 \theta$ and thus the number of DOF is 39. In Table V we present the best-fit values of parameters, χ_{min}^2 and the goodness of fit (GOF) of the solutions for both BP2000 and seismic model for $\nu_e - \nu_{\text{active}}$ transitions. There are five allowed solution in both models – Large Mixing Angle (LMA), Vacuum Oscillation (VO), Low Δm^2 - Quasivacuum Oscillation (LOW-QVO), Just So² [48] and Small Mixing Angle (SMA) – in order of decreasing GOF. The GOF in these regions are more or less similar in both models. The best-fit for both models comes in the LMA region. In order to understand the results of Table V, we write Eq. (13) as

$$P_{ee} = P^D - \frac{1}{\epsilon}(2P^D - 1)f_{\text{reg}} \quad (19)$$

with $\epsilon = \cos 2\theta$, $f_{\text{reg}} = |A_{2e}^\oplus|^2 - \sin^2 \theta$ and P^D defined above in Eq. (14). In Fig. 1 we plot the regeneration factor f_{reg} and the actual Earth regeneration $R_E = P_{ee} - P^D$ vs. energy at the SK latitude for the best-fit values of parameters in the SMA, LMA and LOW regions. Since the latitude of the other detectors are not very different we do not expect f_{reg} and R_E to be very different for these. Since f_{reg} is always positive, the possibility of regeneration inside the Earth depends on P_J . For $P_J < \frac{1}{2}$ there is ν_e regeneration inside Earth while for $P_J > \frac{1}{2}$ more ν_e 's are flavor converted.

- For the SMA region $\epsilon \approx 1$ and from Fig. 1 we observe that f_{reg} is very small excepting for two peaks at $E \approx 6$ MeV and $E \approx 15$ MeV corresponding to strong enhancement of the earth regeneration effect for the neutrinos passing through the core [49,42]. Hence

$$P_{ee}^{\text{SMA}} \approx P^D \quad (20)$$

In this region for low energy (pp) neutrinos, resonance is not encountered (resonance density \gg maximum solar density) and hence $P_J \approx 0$ and $\cos 2\theta_m \approx 1$ giving $P_{ee}^{\text{SMA}} \approx 1$. For intermediate energy (${}^7\text{Be}$) neutrinos $\cos 2\theta_m \approx -1$ (resonance density \ll production density) and $P_{ee}^{\text{SMA}} \approx P_J \approx 0$ for these energies. For high energy (${}^8\text{B}$) neutrinos also, $\cos 2\theta_m \approx -1$ and $P_{ee}^{\text{SMA}} \approx P_J$, with P_J rising with energy. This energy dependence of the SMA survival probability gives a GOF of 9.22% for BP2000 and 9.21% for the seismic model for a simultaneous description of all the four observed rates given in Table IV and the SK spectrum.

- For the Δm^2 of the LMA solution in Table V, the motion of the neutrino in the solar matter is adiabatic for almost all neutrino energies and $P_J \approx 0$. For low energy neutrinos the matter effects are weak both inside the Sun and in Earth giving $f_{\text{reg}} \approx 0$ and $\cos 2\theta_m \approx \epsilon$ so that for Ga energies [51]

$$P_{ee}^{\text{LMA}} \approx \frac{1}{2}(1 + \epsilon^2) \quad (21)$$

At SK and SNO energies matter effects result in $\cos 2\theta_m \approx -1$ while f_{reg} is small but non-zero (≈ 0.03 at 10 MeV as seen from fig. 1) giving

$$\begin{aligned} P_{ee}^{\text{LMA}} &\approx \frac{1}{2}(1 - \epsilon) + f_{\text{reg}} \\ &= \sin^2 \theta + f_{\text{reg}} \end{aligned} \quad (22)$$

With the values of ϵ from Table V and f_{reg} given in fig. 1 eqs. (21) and (22) approximately reproduce the rates of Table IV. Since the probability (22) is approximately energy independent it can account for the flat recoil electron energy spectrum. Since the seismic model predicts a higher value for observed to predicted ratio for the SK, SNO and Cl rates, the best-fit value of $\sin^2 \theta$ or $\tan^2 \theta$ obtained for seismic model are larger (cf. Eq. (22)).

- In the LOW region $\cos 2\theta_m \approx -1$ for all neutrino energies and $P_J \approx 0$ (except for very high energy neutrinos) and thus

$$P_{ee}^{\text{LOW}} = \frac{1}{2}(1 - \epsilon) + f_{\text{reg}} \quad (23)$$

As is seen from Fig. 1 f_{reg} is small for high energy neutrinos and large for low energy neutrinos. For the best-fit case $\epsilon = 0.2$ and $f_{\text{reg}} \sim 0.2$ for Ga energies and ~ 0.025 for SK energies, which can just about reconcile the Ga and SK rates. But it provides a very good description of the flat SK spectrum. The best-fit mixing angle is larger for the seismic case as in LMA.

- At the best-fit value of Δm^2 of Table V for VO solutions the energy smearing over the bins washes out the energy variation due to the oscillations and the flat recoil electron spectrum observed at SK can be explained.
- For the Δm^2 in the Just So² region one gets a very small survival probability for the ⁷Be neutrinos while for the ⁸B neutrinos the survival probability is close to 1.0 [52]. Therefore it cannot explain the total rates data but since it gives a flat probability for the ⁸B neutrinos the spectrum shape can be accounted for and the global analysis gives a GOF of 8.1% in BP2000 and 12.49% in seismic. Since the ratios of observed rates to predicted rates are higher for seismic Just So² gives a lower contribution to χ_{rates}^2 and a better GOF in seismic.

In Fig. 2 we plot the 90% ($\chi^2 \leq \chi_{\text{min}}^2 + 4.61$), 95% ($\chi^2 \leq \chi_{\text{min}}^2 + 5.99$), 99% ($\chi^2 \leq \chi_{\text{min}}^2 + 9.21$) and 99.73% C.L. ($\chi^2 \leq \chi_{\text{min}}^2 + 11.83$) allowed areas in the $\Delta m^2 - \tan^2 \theta$ plane for both BP2000 and the seismic model. We plot the allowed regions with respect to the *global minimum*. Both the models do not admit any allowed area in the SMA region. For other regions the allowed areas in SSM and seismic model are roughly similar with the following differences observed in the seismic case:

- more area seems to be allowed in the LMA and LOW-QVO region
- the LMA region extends to higher Δm^2
- higher values of mixing angles are allowed for LMA and LOW-QVO regions, specifically, with LMA extending into the dark zone ($\theta > \pi/4$).

For the Ga experiment, the seismic model predicts a higher pp and lower ⁸B flux as compared to BP2000. The net effect is that the increase of the flux ratio is smaller in Ga than in SNO, SK and Cl and the observed to predicted rate in Ga is closer to that in Cl, SK and SNO for the seismic model. Thus the energy dependence between the low energy pp and high energy ⁸B rates seen for BP2000 is reduced in the seismic model and the data can now be better accounted by an energy independent scenario. In fact, since the energy distortion in the observed rate is less in the seismic case, most parts of the bands in the parameter space with energy dependence of $< 10\%$ are permitted³. This accounts for the

³ Figure 1 of reference [23].

extended allowed areas appearing in Fig. 2 for the seismic model. These extended areas with weak energy dependence include both high Δm^2 zones as well as high mixing angles⁴. In fact, the allowed area expands well into the dark zone for the LMA solution. For these values of the mixing angles the predicted flux ratio for the SK and SNO is more than that for Ga, against the energy trend of the data. However, for the seismic model these zones are still allowed at 99.73% C.L. owing to the proximity of the Ga and SK-SNO rates.

In Fig. 3a and Fig. 3b we show the experimental rates with their 3σ errors, together with the 3σ range of predicted rates for the LMA (Fig. 3a) and LOW-QVO-VO (Fig. 3b) solutions, in the plane of any two experiments taken together. From the figures it is clear that the LMA (LOW-QVO) region can better account for the SSM(seismic model) predicted rates.

In Table VI we give the χ^2_{\min} and the best-fit points for ν_e transition to sterile neutrino. Since the ^8B flux measured by the charged current reaction at SNO is significantly lower than the observed SK flux, all the sterile solutions appear to be disfavored with more than 90% probability, except for the VO solution for BP2000 and both VO and Just So² for the seismic model. The VO solution produces better fits than the MSW solutions as it gives a lower contribution to the χ^2_{spectrum} (cf.eq. (16)). As in the $\nu_e - \nu_{\text{active}}$ case, Just So² gives a better fit for seismic.

V. CONCLUSIONS

The measured solar neutrino fluxes have been consistently lower than the theoretical predictions from SSM. We have constructed a seismic model of the sun consistent with the helioseismic data that predicts ^8B fluxes lower than that predicted by BP2000, but the corresponding pp flux turns out to be slightly higher in the seismic model. We examine how the use of the seismic model fluxes changes quality of the fits in the MSW and the vacuum oscillation region as compared to BP2000. For the statistical analysis of the data we use a χ^2 minimization technique where we vary the normalization of the spectrum as a free parameter and thus avoid the over-counting of the SK observed flux and consider only the shape information from the SK spectral data. We find that the inclusion of theoretical uncertainties and their correlations self consistently in both models result in fairly similar GOF for the oscillation solutions in both models. However, we note that the use of seismic fluxes does modify the allowed areas in the parameter space. The increased proximity of the Ga and SK rates reduces the energy distortion of the observed fluxes and allows the regions of parameter space with weak energy dependence.

ACKNOWLEDGMENTS

This work utilizes data from the Solar Oscillations Investigation/ Michelson Doppler Imager (SOI/MDI) on the Solar and Heliospheric Observatory (SOHO). The MDI project

⁴ The increase of the mixing angle with the decrease of the gap between the Ga and SK-SNO rates can also be inferred by comparing Eq. (21) and (22).

is supported by NASA grant NAG5-8878 to Stanford University. SOHO is a project of international cooperation between ESA and NASA. SMC wishes to express his thanks to the Leverhulme Trust for the award of a Visiting Professorship at Queen Mary College, London. We thank Prof. S.T. Petcov for his comments.

REFERENCES

- [1] Q.R. Ahmad *et al.*, <http://www.sno.phy.queennsu.ca/sno/firstresults/>, nucl-ex/0106015.
- [2] Y. Fukuda *et al.* (The Super-Kamiokande collaboration), Phys. Rev. Lett. **81**, 1158 (1998); erratum **81**, 4279 (1998);
- [3] B.T. Cleveland *et al.* Astrophys. J **496**, 505 (1998).
- [4] Y. Fukuda *et al.*, (The Kamiokande collaboration), Phys. Rev. Lett. **77**, 1683 (1996).
- [5] J.N. Abdurashitov *et al.*, (The SAGE collaboration), Phys. Rev. Lett. **77**, 4708 (1996); Phys. Rev. **C 60**, 055801 (1999); W. Hampel *et al.*, (The Gallex collaboration), Phys. Lett. **B388**, 384 (1996); Phys. Lett. **bf B447**, 127 (1999); Talk presented in Neutrino 2000 held at Sudbury, Canada (T.A. Kirsten for The Gallex collaboration), Nucl. Phys. **B Proc. Suppl. 77**, 26 (2000); M. Altmann *et al.*, (The GNO collaboration), Phys. Lett. **bf B492**, 16 (2000); Talk presented in Neutrino 2000 held at Sudbury, Canada (E. Bellotti for the GNO Collaboration) Nucl. Phys. **B Proc. Suppl. 91** 44 (2001).
- [6] J.N. Bahcall, N.A. Bahcall, G. Shaviv, Phys. Rev. Lett. **20**, 1209 (1968); J.N. Bahcall and Ulrich (1988); J.N. Bahcall, M.P. Pinsonneault, Rev. Mod. Phys. **64**, 885 (1992); J.N. Bahcall and M.H. Pinsonneault, Rev. Mod. Phys. **67**, 781 (1995).
- [7] J.N. Bahcall, S. Basu, M.P. Pinsonneault, Phys. Lett. **B433**, 1 (1998).
- [8] J.N. Bahcall, S. Basu, M. Pinsonneault, Ap. J. **555**, 990 (2001).
- [9] D.O. Gough, *et al.*, Science, **272**, 1296 (1996).
- [10] H. Shibahashi and M. Takata, PASJ, **48**, 377 (1996).
- [11] H.M. Antia and S.M. Chitre, A&A, **339**, 239 (1998).
- [12] H.M. Antia and S.M. Chitre S. M., MNRAS, **289**, L1 (1997).
- [13] S. Degl’Innocenti, G. Fiorentini and B. Ricci, Phys. Lett. **B416**, 365 (1998).
- [14] H.M. Antia and S.M. Chitre, A&A, **347**, 1000 (1999).
- [15] H. Schlattl, A. Bonanno and L. Paternó, Phys. Rev. **D60**, 113002 (1999).
- [16] Y. Fukuda *et al.* (The Super-Kamiokande collaboration), Phys. Rev. Lett. **82**, 2430 (1999).
- [17] Y. Fukuda *et al.* (The Super-Kamiokande collaboration), Phys. Rev. Lett. **82**, 1810 (1999).
- [18] J.N. Bahcall, P.I. Krastev, and A.Yu. Smirnov, Phys. Rev. **D58**, 096016 (1998).
- [19] M.C. Gonzalez-Garcia and C. Peña-Garay, Nucl. Phys. Proc. Suppl. **91**, 80 (2000); M.C. Gonzalez-Garcia, P.C. de Holanda, C. Peña-Garay, and J.W.F. Valle, hep-ph/9906469, Nucl. Phys. **B573**, 3 (2000).
- [20] S. Goswami, D. Majumdar and A. Raychaudhuri, hep-ph/9909453.
- [21] S. Goswami, D. Majumdar and A. Raychaudhuri, Phys. Rev. **D63**, 013003, (2001).
- [22] J.N. Bahcall, P.I. Krastev, and A.Yu. Smirnov, hep-ph/0103179.
- [23] S. Choubey, S. Goswami, N. Gupta and D.P. Roy, Phys. Rev. **D64**, 053002, (2001).
- [24] G.L. Fogli, E. Lisi, D. Montanino and A. Palazzo, hep-ph/0106247.
- [25] J.N. Bahcall, M.C. Gonzalez-Garcia and C. Peña-Garay, hep-ph/0106258.
- [26] A. Bandyopadhyay, S. Choubey, S. Goswami and K. Kar, hep-ph/0106264.
- [27] P. Creminelli, G. Signorelli, A. Strumia, hep-ph/0102234.
- [28] Y. Fukuda *et al.*, Phys. Rev. Lett. **86**, 5651 (2001).
- [29] E.J. Rhodes, A.G. Kosovichev, J. Schou, P.H. Scherrer and J. Reiter Solar Phys. **175**, 287 (1997).
- [30] H.M. Antia, A&A, **307**, 609 (1996).

- [31] O. Richard, S. Vauclair, C. Charbonnel and W.A. Dziembowski, *A&A*, **312**, 1000 (1996).
- [32] C.A. Iglesias and F.J. Rogers, *ApJ*, **464**, 943 (1996).
- [33] F.J. Rogers, F.J. Swenson and C.A. Iglesias, *ApJ*, **456**, 902 (1996).
- [34] E.C. Adelberger, *Rev. Mod. Phys.* **70**, 1265 (1998).
- [35] S. Basu, *MNRAS*, **298**, 719 (1998).
- [36] A.S. Brun, S. Turck-Chièze and P. Morel, *ApJ*, **506**, 913 (1998).
- [37] A.S. Brun, S. Turck-Chièze and J.P. Zahn, *ApJ*, **525**, 1032 (1999).
- [38] S. Watanabe and H. Shibahashi, *astro-ph/0105445*.
- [39] S. Basu and H.M. Antia *MNRAS*, **269**, 1137 (1994).
- [40] G.L. Fogli, E.Lisi, D. Montanino and A. Palazzo, *Phys. Rev.* **D62**, 113004, (2000).
- [41] S.T. Petcov, *Phys. Lett.* **B200**, 373 (1988).
- [42] S.T. Petcov, *Phys. Lett.* B434, 321 (1998); M. Narayan, G. Rajasekharan and R. Sinha, *Mod. Phys. Lett.* **A13**, 1915 (1998).
- [43] S.T. Petcov, *Phys. Lett.* B214 (1988) 139; *Phys. Lett.* B406, 355 (1997), S.T. Petcov and J. Rich *PL B214*, 137 , (1989).
- [44] A.de. Gouvea, A. Friedland, H. Murayama, *Phys.Lett.***B490**, 125, (2000).
- [45] L. Wolfenstein, *Phys. Rev.* **D34**, 969 (1986); S.P. Mikheyev and A.Yu. Smirnov, *Sov. J. Nucl. Phys.* **42(6)**, 913 (1985); *Nuovo Cimento* **9c**, 17 (1986).
- [46] B. Pontecorvo, *Sov. Phys. JETP* **6**, 429 (1958); V.N. Gribov, B. Pontecorvo, *Phys. Lett.* bf B28, 493 (1969).
- [47] E. Lisi *et al.*, *Phys. Rev.* **D63** 093002, (2001).
- [48] R. S. Raghavan, *Science* **267**, 45 (1995); P.I. Krastev and S.T. Petcov, *Phys. Rev.* **D53**, 1665 (1996).
- [49] E.K. Akhmedov, *Nucl. Phys.* **B538**, 25, (1999).
- [50] G.L. Fogli and E. Lisi, *Astropart. Phys.*, **3**, 185 (1995).
- [51] M.C. Gonzalez-Garcia, C. Peña-Garay, Y. Nir and A. Yu. Smirnov, *Phys. Rev.* **D63**, 013007 (2001).
- [52] See Fig. 5 of [22].

TABLES

TABLE I. Neutrino fluxes in seismic model

Neutrino	Flux, F_ν ($\text{cm}^{-2} \text{ s}^{-1}$)	Logarithmic derivatives $\frac{\partial \ln F_\nu}{\partial \ln X}$						
		$S_{3,3}$	$S_{3,4}$	$S_{1,14}$	$S_{1,7}$	L_\odot	Z	κ
pp	$(6.12 \pm 0.01) \times 10^{10}$	0.03	-0.07	-0.02	0.00	0.96	-0.06	-0.13
pep	$(1.45 \pm 0.01) \times 10^8$	0.03	-0.07	-0.02	0.00	0.76	-0.17	-0.31
hep	$(2.12 \pm 0.01) \times 10^3$	-0.41	-0.07	-0.01	0.00	0.09	-0.21	-0.41
^7Be	$(4.54 \pm 0.12) \times 10^9$	-0.44	0.95	0.00	0.00	2.06	0.68	1.45
^8B	$(4.16 \pm 0.26) \times 10^6$	-0.49	1.04	0.01	1.00	3.85	1.65	3.40
^{13}N	$(5.02 \pm 0.25) \times 10^8$	-0.08	0.14	0.85	0.00	2.39	1.24	2.52
^{15}O	$(4.14 \pm 0.26) \times 10^8$	-0.09	0.17	1.00	0.00	2.93	1.52	3.07
^{17}F	$(4.77 \pm 0.32) \times 10^6$	-0.10	0.18	0.01	0.00	3.07	1.59	3.21
Rel. error		0.060	0.094	0.143	0.11	.004	0.033	0.02

TABLE II. Predicted neutrino fluxes in various solar neutrino experiments

Experiment	Homestake (^{37}Cl) (SNU)	SK (H_2O) ($10^6 \text{ cm}^{-2} \text{ s}^{-1}$)	Gallex, SAGE, GNO (^{71}Ga) (SNU)	SNO CC (D_2O) ($10^6 \text{ cm}^{-2} \text{ s}^{-1}$)
Measured Flux	2.56 ± 0.23	2.32 ± 0.08	74.7 ± 5.0	1.75 ± 0.14
SSM (BP00)	$7.6^{+1.3}_{-1.1}$	$5.05^{+1.01}_{-0.81}$	128.0^{+9}_{-7}	$5.05^{+1.01}_{-0.81}$
SSM (BP95)	$9.3^{+1.2}_{-1.4}$	$6.62^{+0.93}_{-1.13}$	137^{+8}_{-7}	$6.62^{+0.93}_{-1.13}$
SSM (BP98)	$7.7^{+1.2}_{-1.0}$	$5.15^{+0.51}_{-0.72}$	129^{+8}_{-6}	$5.15^{+0.51}_{-0.72}$
SSM (Bru98)	7.2	4.8	127	4.8
SSM (Bru99)	6.7	4.7	125	4.7
Seismic model	6.46 ± 0.99	4.16 ± 0.76	124.9 ± 6.5	4.16 ± 0.76

TABLE III.

The seismic model predictions for the solar neutrinos fluxes and neutrino capture rates in the Cl and Ga detectors. The expected ^8B flux in SK and SNO is as given in Table II.

source	seismic		BP2000	
	^{37}Cl	^{71}Ga	^{37}Cl	^{71}Ga
	(SNU)	(SNU)	(SNU)	(SNU)
pp	0.00	71.58	0.00	69.7
pep	0.23	2.95	0.22	2.8
hep	0.04	0.07	0.04	0.1
^7Be	1.09	32.57	1.15	34.2
^8B	4.74	9.98	5.76	12.1
^{13}N	0.09	3.03	0.09	3.4
^{15}O	0.27	4.72	0.33	5.5
^{17}F	0.00	0.05	0.00	0.1
Total	6.46	124.94	7.6	128.0

TABLE IV. The observed rates relative to the theoretical predictions for Ga, Cl, SK and SNO experiments along with their compositions(comp.) for both seismic model and SSM. The Ga rate corresponds to the combined SAGE and GALLEX+GNO data.

Model	Experiment	Ga	Cl	SK	SNO (CC)
BP2000	Rate	0.584 ± 0.039	0.337 ± 0.030	0.459 ± 0.017	0.347 ± 0.027
	Comp.	pp (55%), ^7Be (25%), ^8B (10%)	^7Be (15%), ^8B (75%)	^8B (100%)	^8B (100%)
SEISMIC	Rate	0.598 ± 0.040	0.396 ± 0.035	0.557 ± 0.021	0.421 ± 0.033
	Comp.	pp (57%), ^7Be (26%), ^8B (8%)	^7Be (17%), ^8B (73%)	^8B (100%)	^8B (100%)

TABLE V. The best-fit values of the parameters, χ^2_{\min} , and the goodness of fit from the global analysis of rates and the 1258 day SK day-night spectrum data for MSW analysis involving two active neutrino flavors.

	Nature of Solution	Δm^2 in eV^2	$\tan^2 \theta$	χ^2_{\min}	Goodness of fit
BP2000	SMA	5.28×10^{-6}	3.75×10^{-4}	51.14	9.22%
	LMA	4.70×10^{-5}	0.38	33.42	72.18%
	LOW-QVO	1.76×10^{-7}	0.67	39.00	46.99%
	VO	4.64×10^{-10}	0.57	38.28	50.25%
	Just So ²	5.37×10^{-12}	0.77	51.90	8.10%
SEISMIC	SMA	4.66×10^{-6}	5.10×10^{-4}	51.15	9.21%
	LMA	5.11×10^{-5}	0.44	35.62	62.48%
	LOW-QVO	1.76×10^{-7}	0.71	38.22	50.53%
	VO	4.65×10^{-10}	0.47	36.23	59.69%
	Just So ²	5.37×10^{-12}	1.00	49.30	12.49%

TABLE VI. The The best-fit values of the parameters, χ^2_{\min} , and the goodness of fit from the global analysis of rates and the 1258 day SK day-night spectrum data for two-generation $\nu_e - \nu_{\text{sterile}}$ MSW analysis.

	Nature of Solution	Δm^2 in eV^2	$\tan^2 \theta$	χ^2_{\min}	Goodness of fit
BP2000	SMA	5.59×10^{-6}	2.83×10^{-4}	54.21	5.35%
	LMA	6.13×10^{-5}	0.50	52.93	6.75%
	LOW-QVO	2.93×10^{-8}	1.00	53.18	6.46%
	VO	4.67×10^{-10}	0.37	46.28	19.70%
	Just So ²	5.37×10^{-12}	0.77	52.09	7.83%
SEISMIC	SMA	3.81×10^{-6}	3.67×10^{-4}	58.18	2.47%
	LMA	6.04×10^{-5}	0.62	54.97	4.64%
	LOW-QVO	3.20×10^{-8}	1.00	53.26	6.36%
	VO	4.68×10^{-10}	0.37	44.82	24.09%
	Just So ²	5.37×10^{-12}	0.98	49.51	12.07%

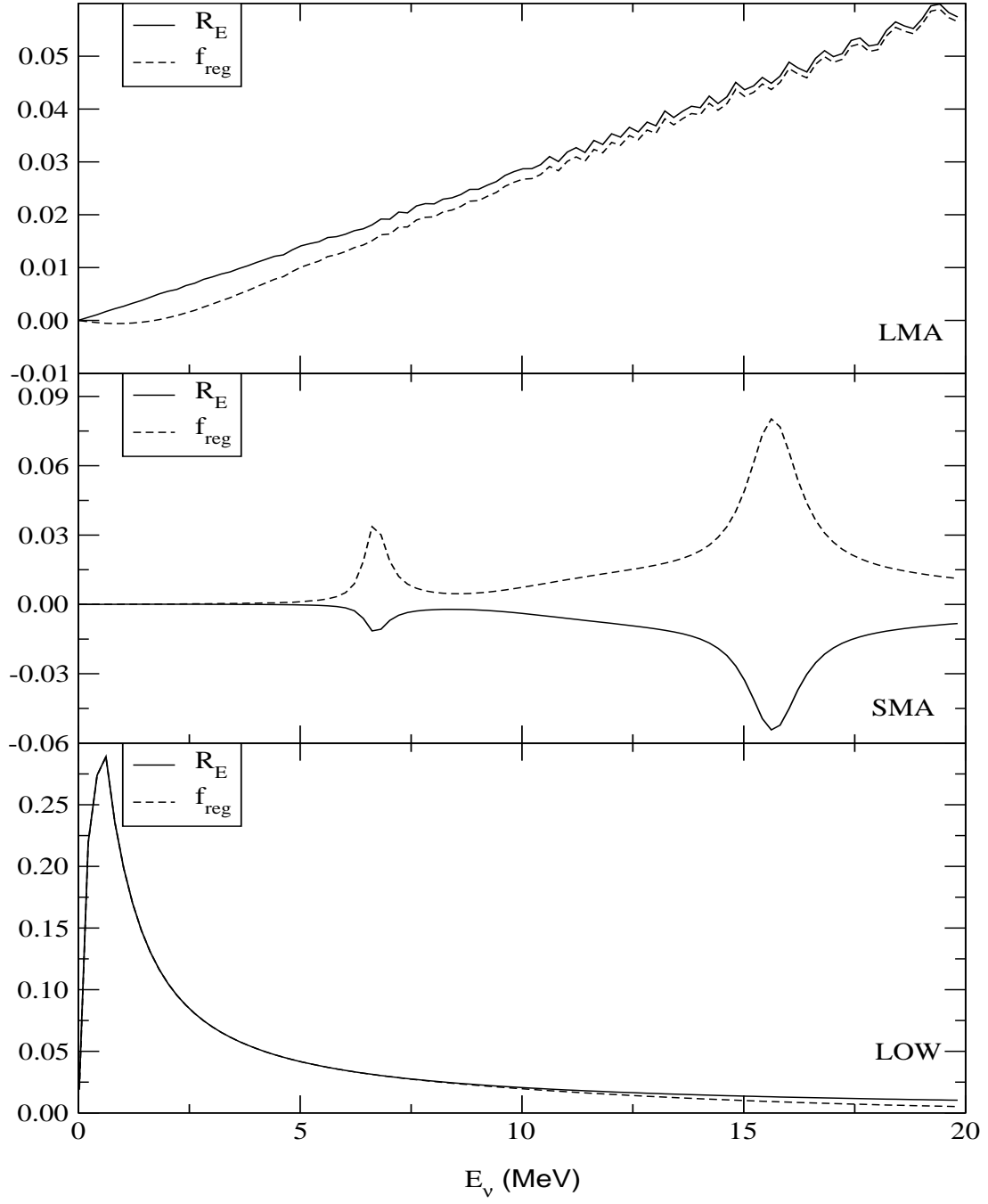


Fig. 1: The regeneration factor $f_{\text{reg}} = (|A_{2e}|^2 - \sin^2 \theta)$ and the net Earth regeneration $R_E (= P_{ee} - P^D)$ as a function of energy for typical values of the parameters in the SMA, LMA and LOW-QVO regions.

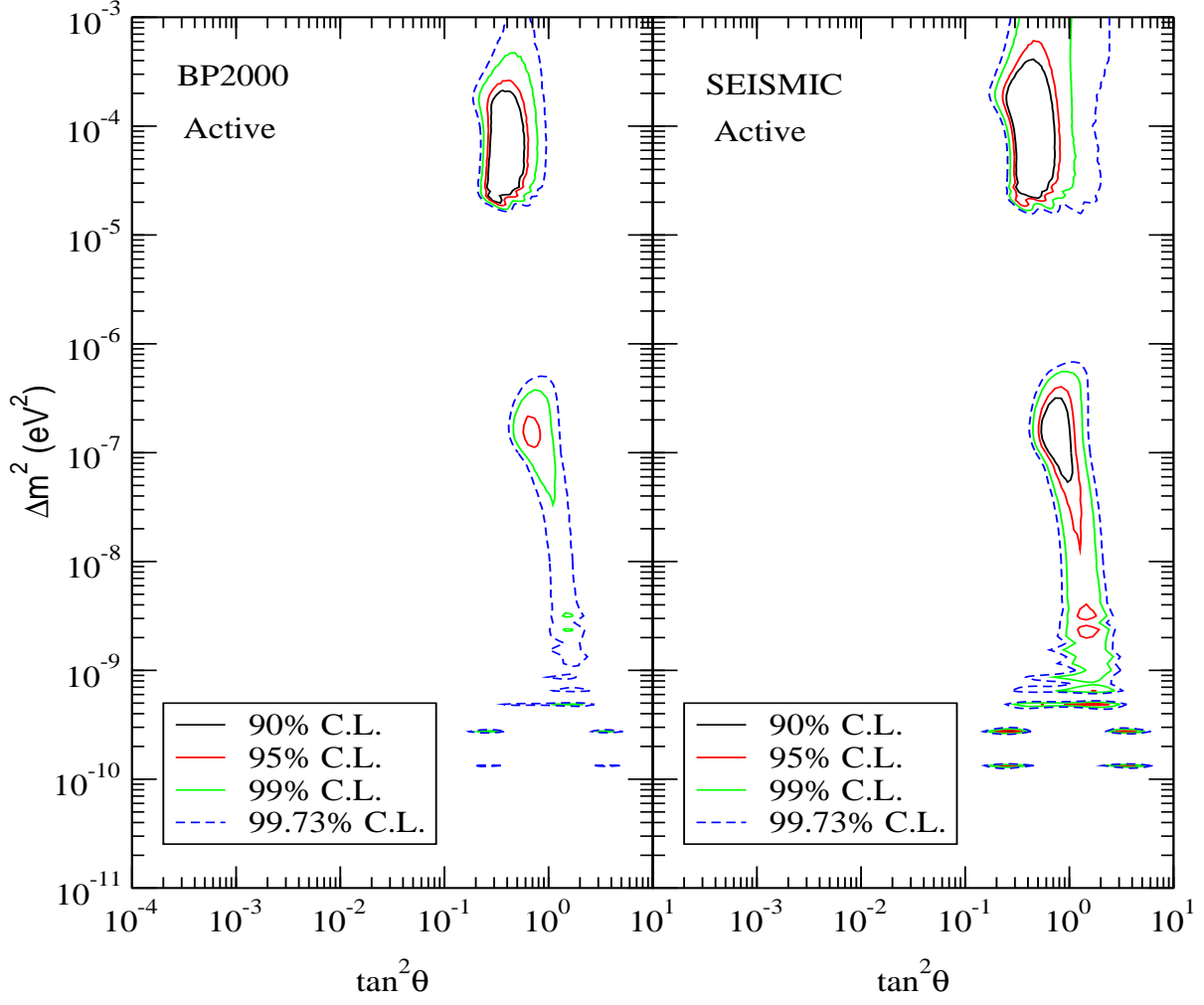


Fig. 2: The 90%, 95%, 99% and 99.73% C.L. allowed areas from the global analysis of the total rates from Cl, Ga, SK and SNO detectors and the 1258 day SK recoil electron spectrum at day and night, assuming MSW conversions to active neutrinos, using theoretical predictions from BP2000 and seismic model.

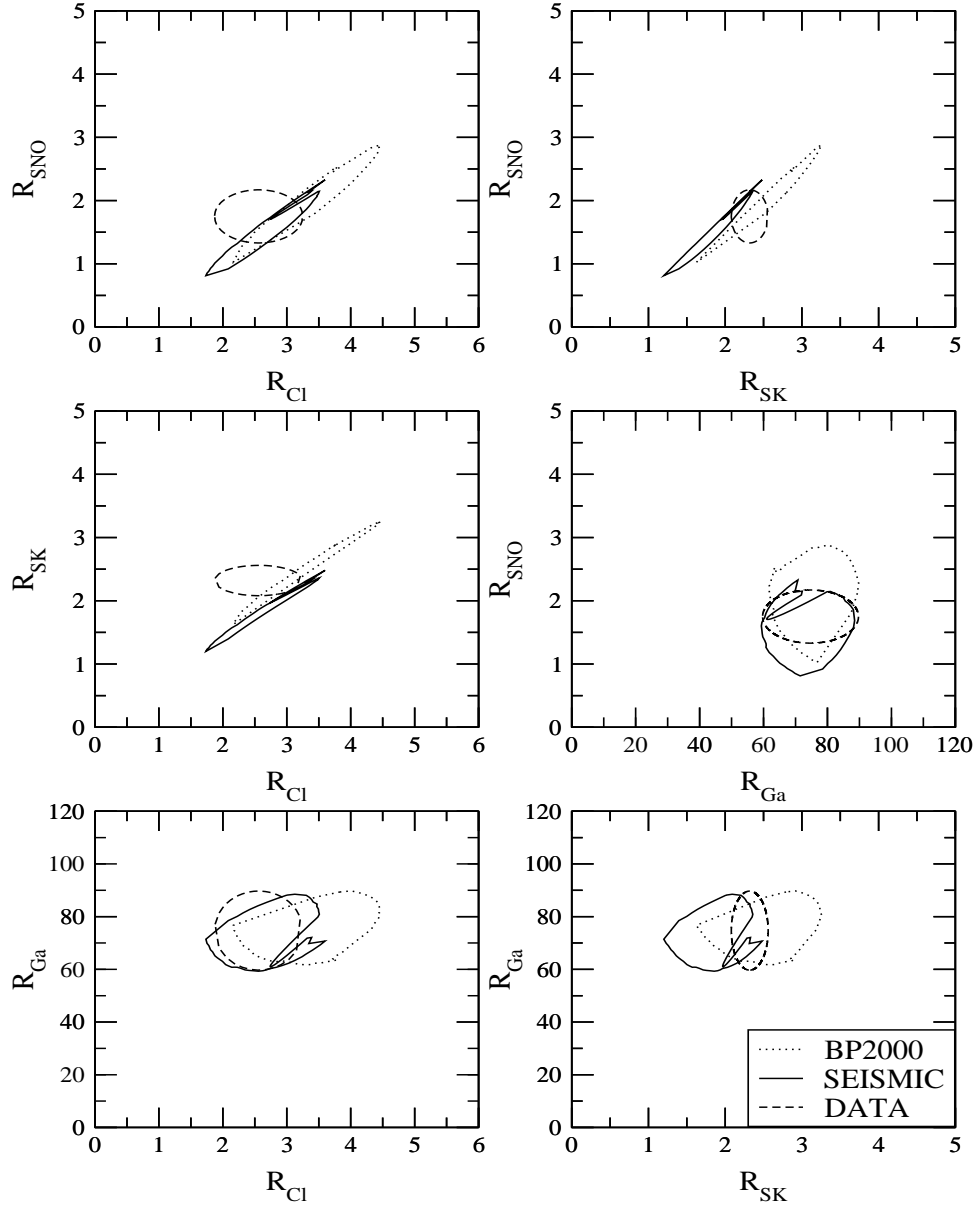


Fig. 3a: The experimental rates (in SNU for the Cl and Ga experiments and in units of $10^6 \text{ cm}^{-2} \text{ s}^{-1}$ for SK and SNO) with 3σ errors (shown by ellipses) and the 99.73% C.L. range of predicted rates for LMA solution, in the plane of any two of the experiments for BP2000 (dotted line) and for seismic model (solid line).

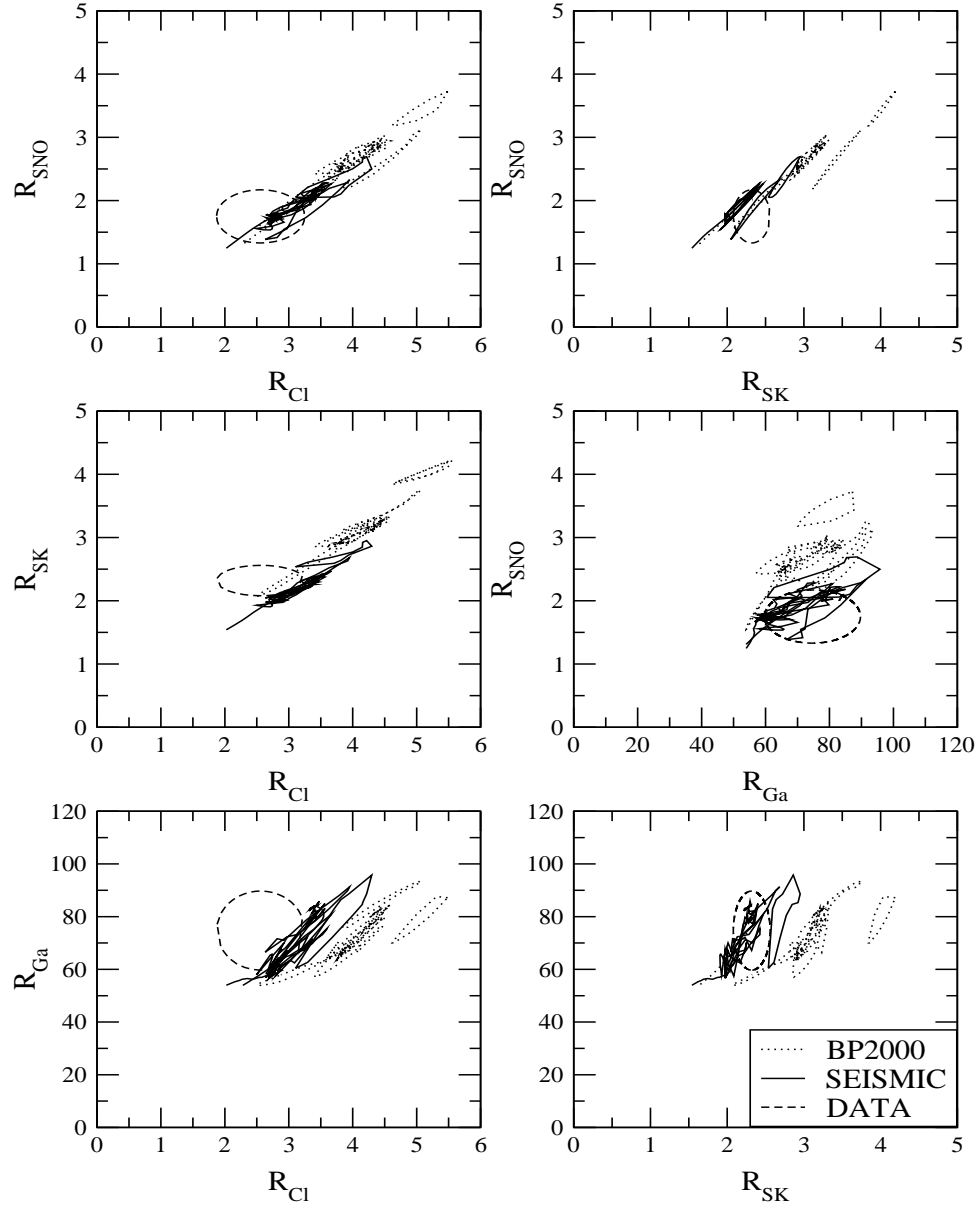


Fig. 3b: same as in fig. 3a but for LOW-QVO-VO solution. For this solution there are multiple contours (cf. Fig. 2), resulting in a complicated pattern.